An Efficient Tool for Multi-Frequency Analysis in Acoustic Scattering or Radiation by Boundary Element Method

Christian Vanhille, Antoine Lavie

© S. Hirzel Verlag · EAA
ACUSTICA · acta acustica
Vol. 84 (1998) 884–893

An Efficient Tool for Multi-Frequency Analysis in Acoustic Scattering or Radiation by Boundary Element Method

Christian Vanhille, Antoine Lavie*

Institut d'Electronique et de Microélectronique du Nord, U.M.R. C.N.R.S. 9929, Département I.S.E.N., Laboratoire d'Acoustique, 41 Boulevard Vauban, 59046 Lille Cédex, France

Summary

In this article, a new boundary element algorithm in acoustic scattering or radiation is proposed. Based upon a linear frequency interpolation, this original method allows a real practical, fast and easy use of the boundary element method for a multi-frequency analysis. This technique is original for two reasons. The first one is the automation of its utilization using the interpolation between the two bounding frequencies 0 Hz and the top-frequency of the spectrum, given by the "$\lambda/4$ criterion" associated with the quadratic isoparametric discretization for any geometry. Furthermore, in the case of its application to axisymmetrical problems, the circular surface elements of the mesh are automatically split through decomposition points. This allows a saving of central processor unit time. Moreover, this profit increases very quickly with the size of the mesh and the number of calculation frequencies. These motives make this boundary element linear interpolation method very attractive.

PACS no. 43.20.Fn, 43.20.Tb, 43.30.Jx, 43.40.Rj

1. Introduction

The problem which has justified the study presented here is the resolution of the radiation problem from a vibrating structure with prescribed surface displacements or the scattering problem of a target impinged by an incident wave and immersed in a fluid medium of infinite extension. This fluid-structure coupling problem is modelled using two numerical codes via impedance matrices: the EQI code applied to the propagation in the fluid medium with a boundary element method (BEM) and the ATILA code [1, 2] applied to the elastic structure behaviour with a finite element method. The EQI code has been validated for solving radiation and scattering problems by comparisons with analytical solutions and experimental results [3, 4, 5, 6, 7, 8, 9, 10].

The BEM has been for about 30 years an usual and good numerical technique for acoustic analysis. The most notable feature of the BEM is that only the boundary (surface) of a three-dimensional body (or cavity) is modelled in order to obtain a numerical solution. Even for exterior problems of infinite extent, the BEM discretization limited to the finite boundary of the body, by invoking implicitly the Sommerfeld radiation condition, allows to model completely the propagation in the fluid. In this case, this method is more efficient than the finite element method that requires meshing of a part of the surrounding medium with appropriated damped conditions on the boundary of the fluid mesh [1, 2]. For this reasons, the coupling between the EQI and ATILA codes is a powerful tool to analyse fluid-structure problems. Another advantage of the BEM is its ability to study complex geometrical structures.

Received 30 January 1996,
accepted 12 November 1997.

* Present address:
Laboratoire d'Artois, Mécanique et Habitat, Université d'Artois, Technoparc Futura, 62 400 Béthune, France

The major drawback of the BEM is the presence of irregular frequencies, for which an infinite number of solutions exists [11]. For an exterior Neumann problem, this mathematical problem occurs at some characteristic frequencies of the associate Dirichlet interior problem [12, 11]. Numerically, this means that at these eigenfrequencies and in their neighbourhood, the matrices become singular. In the EQI code, this drawback is overcome using the Jones method [13, 4]: the integral equations system is overdetermined by null-field equations. The efficiency of the Jones method is not subordinated to the location of the origin of these equations compared to the nodal surfaces of the interior problem [3]. This is due to the possibility to increase the degree of these latest equations.

The BEM needs a lot of central processor unit time (CPU time) divided into two parts: the matrix construction phase and the resolution phase of the integral equations system. For a three-dimensional (3D) resolution, most CPU time is spent in the resolution phase. On the other hand, for an axisymmetrical resolution, most CPU time is spent in the matrix construction phase.

Although the BEM is a very efficient numerical technique for acoustic analysis for a single frequency, it may lose its advantage for a multi-frequency run. The main reason is that the integrals of the coefficients of the system are frequency dependent. For each different frequency, all the components in the coefficient matrices and vectors need to be recalculated. The procedure will be very time consuming if solutions for a wide frequency spectrum are required for analysis.

A way to decrease this multi-frequency difficulty is to use a linear frequency interpolation technique initially proposed by Benthien [14]. The idea is to eliminate the oscillation of the coefficients matrices with the frequency, this oscillation being due to the important variation of the kD term (where k is the wave number and D the influence distance, i.e. distance between the calculation point $\boldsymbol{r}$ and the integration point $\boldsymbol{r}'$)

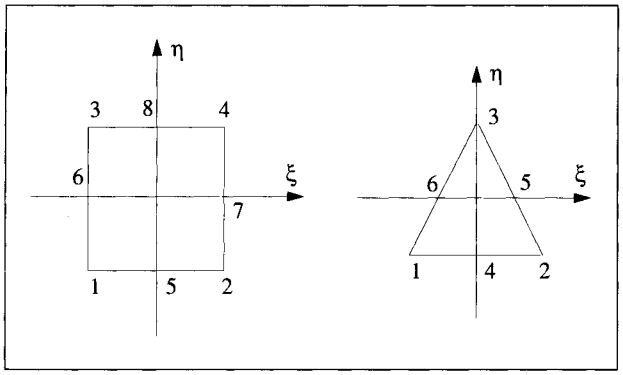

Figure 1. 3D quadratic isoparametric elements, with $-1 \leq \xi \leq 1$, $-1 \leq \eta \leq 1$.

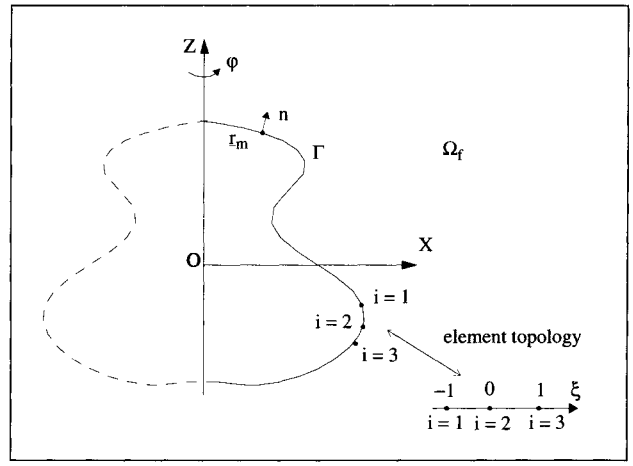

Figure 2. Axisymmetrical quadratic isoparametric element.

in the exponential term of the free-space Green's function:

$$g(\boldsymbol{r}, \boldsymbol{r}') = \frac{1}{4\pi} \frac{\mathrm{e}^{ikD}}{D}. \tag{1}$$

By extracting a quantity close to kD from the exponential, a very slow frequency variation coefficient is obtained. So, a linear frequency interpolation can be carried out at a calculation frequency situated between two storage frequencies, called bounding frequencies, the original coefficient being recovered after multiplying by the sinusoidal oscillating term.

This technique widely differs according to the type of discretization used. Its first implementation was based on constant elements [14]. This technique has been extended to quadratic isoparametric elements [15, 16, 17] in the case of 3D problems without considering the axisymmetrical case.

The subject of this paper deals with the fluid propagation part of this coupling, i.e. the BEM code, and, in particular, with a multi-frequency analysis development. In this case, the boundary conditions are Neumann conditions (scattering of an incident plane wave by a rigid body or radiation in the fluid from an elastic structure on which displacements are prescribed). The time dependence of the variables (pressure and displacement) is harmonic ($\mathrm{e}^{\mathrm{i}\omega t}$). The linear frequency interpolation method is applied to 3D and axisymmetrical problems with quadratic isoparametric elements. An original way of computing the non-oscillating coefficient is shown in the axisymmetrical case. It consists in decomposing every circular element into sub-circular elements on which an adapted distance is used to factorise out the variation terms in the matrix coefficients. This decomposition leads to an important saving of CPU time.

After a brief reminder of the BEM theory, this article presents the linear frequency interpolation principle and its application to 3D problems. Then, the description of a numerical integration technique and the new multi-frequency analysis applied to the axisymmetrical problems is presented. Finally, numerical validation and conclusions are provided.

All the test have been realised on a HP 9000/735 workstation, the sound speed in the fluid medium (water) is 1490 m/s.

2. Conventional basic equations

In this part, the BEM is briefly reviewed.

The well-known Helmholtz differential equation governs the propagation in linear acoustics:

$$\Delta p + k^2 p = 0 \tag{2}$$

for the high pressure p (called pressure in the following), where k is the wave number. At the same time, Dirichlet or Neumann conditions on the surface of the immersed structure and Sommerfeld condition are taken into account.

Usually, this differential equation with boundary conditions is replaced [18, 19, 11] by the Helmholtz integral equation (HIE):

$$p_{\mathrm{inc}}(\boldsymbol{r}) + \iint_{\Gamma} p(\boldsymbol{r}') \frac{\partial g(\boldsymbol{r}, \boldsymbol{r}')}{\partial n'} - \frac{\partial p(\boldsymbol{r}')}{\partial n'} g(\boldsymbol{r}, \boldsymbol{r}') \, \mathrm{d}\boldsymbol{r}' =$$

$$p(\boldsymbol{r}) \qquad \boldsymbol{r} \in \boldsymbol{\Omega}_f \tag{3}$$

$$\frac{\alpha(\boldsymbol{r})}{4\pi} p(\boldsymbol{r}) \qquad \boldsymbol{r} \in \boldsymbol{\Gamma} \tag{4}$$

where p_{inc} is the incident wave, $\boldsymbol{r}$ the calculation point on the surface $\boldsymbol{\Gamma}$ or in the fluid domain $\boldsymbol{\Omega}_{\mathbf{f}}$, $\boldsymbol{r}'$ an integration point on $\boldsymbol{\Gamma}$, g the free-space Green's function previously defined, $\partial/\partial n'$ the outward normal derivative on the surface at $\boldsymbol{r}'$, $\mathrm{d}\boldsymbol{r}'$ the surface element and α the solid angle. The discretization of the surface equation (4) using isoparametric elements with quadratic variation [20] leads to the linear square system:

$$[A]\{p\} = [B]\left\{\frac{\partial p}{\partial n}\right\} - \{p_{\mathrm{inc}}\}, \tag{5}$$

where $[A]$ and $[B]$ are the integral equations matrices, $\{p\}$, $\{\partial p/\partial n\}$ and $\{p_{\mathrm{inc}}\}$ are the nodal pressures, nodal normal derivative pressures and nodal incident pressure vectors. For the Neumann problem, the unknown is the $\{p\}$ vector. After calculation of the surface pressure, the near-field pressure and the far-field pressure can be directly deduced.

For a 3D problem, respectively for the left-hand and the right-hand matrix, the matrix coefficients of the linear system

ACUSTICA · acta acustica
Vol. 84 (1998)

are [4]:

$$A_{m\,ij} = \iint_{\Gamma_j} \frac{\partial}{\partial n'} g\big(\boldsymbol{r}_m, \boldsymbol{r}'(\xi,\eta)\big) N_i(\xi,\eta)\,\mathrm{d}\boldsymbol{r}'(\xi,\eta) - \delta_{m\,ij}\frac{\alpha_m}{4\pi}, \tag{6}$$

$$B_{m\,ij} = \iint_{\Gamma_j} g\big(\boldsymbol{r}_m, \boldsymbol{r}'(\xi,\eta)\big) N_i(\xi,\eta)\,\mathrm{d}\boldsymbol{r}'(\xi,\eta), \tag{7}$$

where m is the index of the calculation node, ij the index of the node i of the element Γ_j, N_i the pondering functions of the element Γ_j, δ the Kronecker's symbol and (ξ,η) are the local coordinates on the element (see Figure 1). In the case of an axisymmetrical problem, these coefficients are [4]:

$$A_{m\,ij} = \iint_{\Gamma_j} \frac{\partial}{\partial n'} g\big(\boldsymbol{r}_m, \boldsymbol{r}'(\xi,\varphi)\big) N_i(\xi)\,\mathrm{d}\boldsymbol{r}'(\xi,\varphi) - \delta_{m\,ij}\frac{\alpha_m}{4\pi}, \tag{8}$$

$$B_{m\,ij} = \iint_{\Gamma_j} g\big(\boldsymbol{r}_m, \boldsymbol{r}'(\xi,\varphi)\big) N_i(\xi)\,\mathrm{d}\boldsymbol{r}'(\xi,\varphi), \tag{9}$$

where ξ is the local coordinate on the element and φ the azimuthal angle (see Figure 2). The free-space Green's function and its normal derivative are:

$$g(\boldsymbol{r}_m, \boldsymbol{r}') = \frac{1}{4\pi}\frac{\mathrm{e}^{\mathrm{i}kD_m}}{D_m}, \tag{10}$$

$$\frac{\partial}{\partial n'} g\big(\boldsymbol{r}_m, \boldsymbol{r}'\big) = \frac{1}{4\pi}\frac{\mathrm{e}^{\mathrm{i}kD_m}}{D_m^2}\left[\mathrm{i}k - \frac{1}{D_m}\right] \cdot \big(\boldsymbol{r}'(\xi,\eta) - \boldsymbol{r}_m\big)\cdot \boldsymbol{n}', \tag{11}$$

where D_m is the distance between the calculation node $\boldsymbol{r}_m$ and the integration point $\boldsymbol{r}'$ which depends upon the local coordinates.

3. Linear frequency interpolation method

In this section, the linear frequency interpolation method is detailed.

3.1. Aim

A shortcoming of the BEM is the frequency dependence of the integral equation matrices, and therefore, of the matrix coefficients. So, for each desired calculation frequency, an entire execution of the BEM procedure is needed, and, in particular, an execution of the matrix construction phase. This phase computes the matrix coefficients and requires a great number of integrals calculations. For an analysis of a large bandwidth frequency spectrum, this problem becomes acute, the cost of CPU time is very high.

The linear frequency interpolation method allows to reduce the number of matrix construction phases. Only two matrix construction phases are executed, at the two bounding frequencies. Thus it provides an important saving of CPU time. Between these two frequencies, the matrix construction phase is replaced by a linear frequency interpolation of the corresponding matrix coefficients. This technique is very well suited to axisymmetrical modelling for which the matrix construction phase is very time consuming.

3.2. Method

The method is based upon the elimination of the rapid frequency oscillating character of the BEM matrix coefficients in order to use a linear frequency interpolation formula.

The fluctuating character is due to the heavy variations of kDm and is situated in the exponential of the free-space Green's function and its normal derivative:

$$\mathrm{e}^{\mathrm{i}kD_m}. \tag{12}$$

Then, to smooth out this difficulty, a term close to the value of kD_m is factorised out. So, new coefficients, which theoretically vary very slowly with frequency are obtained, at two bounding frequencies, between which the application of a linear frequency interpolation is possible. Then, multiplication by the extracted fluctuating terms at the interpolating frequency recovers the real matrices.

4. Application to three-dimensional problems

Throughout this section, the application of the linear frequency interpolation to 3D problems is shown, when using quadratic isoparametric elements.

4.1. Theoretical application

The first application of the BEM linear frequency interpolation used discretization with constant elements [14]. Every element contains one node located at its centre. So, the factorising distance is the distance between the calculation node r_m and the unique centroid node of the element Γ_j.

Our work concerns the application of this method for any kind of geometry, while using quadratic isoparametric elements [20]. This type of element can be quadrilateral or triangular as shown on Figure 1. The rectangular element is composed of 8 nodes and the shape functions are:

$$\begin{aligned}
N_1(\xi,\eta) &= \tfrac{1}{4}(\xi-1)(1-\eta)(\xi+\eta+1),\\
N_2(\xi,\eta) &= \tfrac{1}{4}(1+\xi)(1-\eta)(\xi-\eta-1),\\
N_3(\xi,\eta) &= \tfrac{1}{4}(1-\xi)(1+\eta)(\eta-\xi-1),\\
N_4(\xi,\eta) &= \tfrac{1}{4}(1+\xi)(1+\eta)(\xi+\eta-1),\\
N_5(\xi,\eta) &= \tfrac{1}{2}(1-\xi^2)(1-\eta),\\
N_6(\xi,\eta) &= \tfrac{1}{2}(1-\eta^2)(1-\xi),\\
N_7(\xi,\eta) &= \tfrac{1}{2}(1-\eta^2)(1+\xi),\\
N_8(\xi,\eta) &= \tfrac{1}{2}(1-\xi^2)(1+\eta).
\end{aligned} \tag{13}$$

The triangular element is composed of 6 nodes and the shape functions are:

$$\begin{aligned} N_1(\xi,\eta) &= \tfrac{1}{8}(2\xi+\eta+1)(2\xi+\eta-1), \\ N_2(\xi,\eta) &= \tfrac{1}{8}(2\xi-\eta+1)(2\xi-\eta-1), \\ N_3(\xi,\eta) &= \tfrac{1}{2}\eta(1+\eta), \\ N_4(\xi,\eta) &= \tfrac{1}{4}(2\xi-\eta+1)(1-2\xi-\eta), \\ N_5(\xi,\eta) &= \tfrac{1}{2}(1+\eta)(2\xi+\eta-1), \\ N_6(\xi,\eta) &= \tfrac{1}{2}(1+\eta)(1-2\xi-\eta). \end{aligned} \quad (14)$$

The factorising distance $D_{m\,ij}$ is the distance between the calculation node $\boldsymbol{r}_m$ and the node i of the element Γ_j. As $D_{m\,ij}$ is always close to the distance D_m of equation (12), the distance $D_m - D_{m\,ij}$ is always small. Therefore, the coefficients of the matrix $[B]$ can be expressed as:

$$B_{m\,ij} = \frac{1}{4\pi} \mathrm{e}^{\mathrm{i}kD_{m\,ij}} \iint_{\Gamma_j} \frac{\mathrm{e}^{\mathrm{i}k(D_m - D_{m\,ij})}}{D_m} \cdot N_i(\xi,\eta)\,\mathrm{d}\boldsymbol{r}'(\xi,\eta) \quad (15)$$

and those of the "new matrix", distinguished by the symbol $\hat{}$, as:

$$\hat{B}_{m\,ij} = \frac{1}{4\pi} \iint_{\Gamma_j} \frac{\mathrm{e}^{\mathrm{i}k(D_m - D_{m\,ij})}}{D_m} N_i(\xi,\eta)\,\mathrm{d}\boldsymbol{r}'(\xi,\eta). \quad (16)$$

The same decomposition is valid for the matrix $[A]$. The solid angle is not subject to the interpolation method since it does not depend upon frequency.

As opposite to discretization with constant elements, the use of quadratic variation interpolation adds two constraints: the respect of the "$\lambda/4$ criterion", which states that the dimension of the largest element of the mesh has to be minor than a quarter of the wavelength to get a good precision in the computations [20]; the duplicity of the normals at the nodes of the mesh. This latest problem is treated by a projection of the right-hand $[B]$ matrix on the three space coordinates [4, 16].

Therefore, the linear frequency interpolation contains three steps (see Figure 3): a first step where the "new matrices" are calculated and stored at the inferior bounding frequency f_1; a second one which is identical but at the superior bounding frequency f_2; and a third step of interpolation at each calculation frequency f included in the $f_1 - f_2$ range.

The method has been implemented for the 3D case in the EQI code. An automation of its use has even been obtained: the bounding interpolation frequencies have been fixed at 0 Hz for f_1 and F for f_2 where F is the maximum frequency permitted by the "$\lambda/4$ criterion".

However, the matrix construction phase CPU time is small compared to the resolution phase of a 3D problem. So, the saving of CPU time is weak. Moreover, the disk storage space taken up by the bounding matrices can be dissuasive.

In the papers of Wu *et al.* [15, 17], the fluctuating distance used is constant for one element (distance computation node-centroid): it then differs from the one used here and theoretically allows less precision; moreover, the technique is only applied to a spherical structure. However, here, it is generalized to every geometric form, and the problem of duplicity of the normals is taken into account [4, 16].

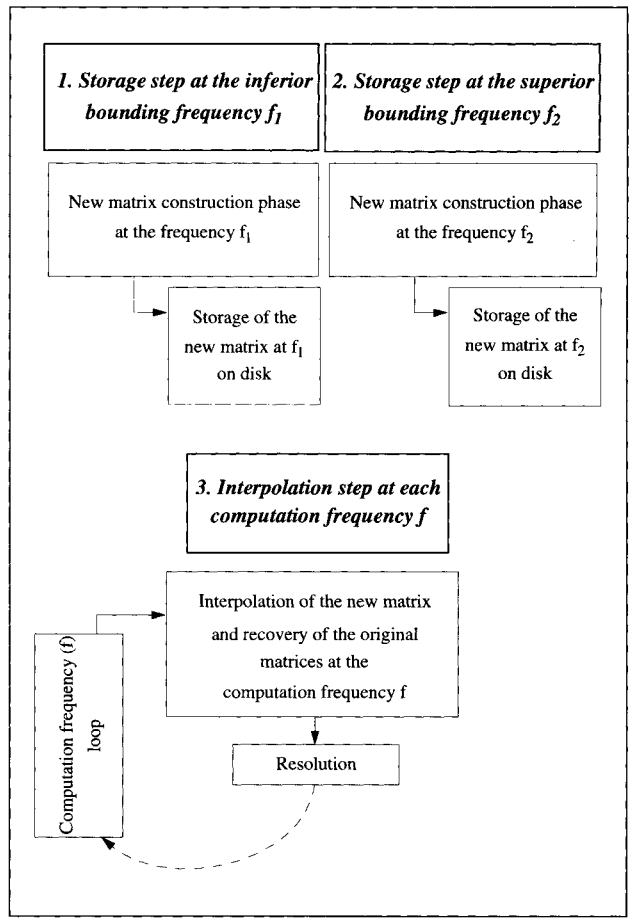

Figure 3. Linear frequency interpolation process.

4.2. Validation

In a classical manner, the numerical validation of the developments is realized using the point-source check [11]. This test consists in situating a point-source into the structure at the point r^0. This source radiates an analytical pressure:

$$p_a(\boldsymbol{r}) = \pm A \frac{\mathrm{e}^{\mathrm{i}k|\boldsymbol{r}-\boldsymbol{r}^0|}}{|\boldsymbol{r}-\boldsymbol{r}^0|} = \pm A \frac{\mathrm{e}^{\mathrm{i}kD}}{D}, \quad (17)$$

from which its normal derivative value is evaluated on the surface:

$$\frac{\partial}{\partial n} p_a(\boldsymbol{r}) = \pm A \frac{\mathrm{e}^{\mathrm{i}kD}}{D^2} \left[\mathrm{i}k - \frac{1}{D}\right] (\boldsymbol{r}^0 - \boldsymbol{r}) \cdot \boldsymbol{n}'. \quad (18)$$

The nodal surface value vector of these derivative values $\{\partial p_a/\partial n\}$ is introduced in the BEM data file. The BEM system is solved in order to obtain the calculated pressure on

ACUSTICA · acta acustica
Vol. 84 (1998)

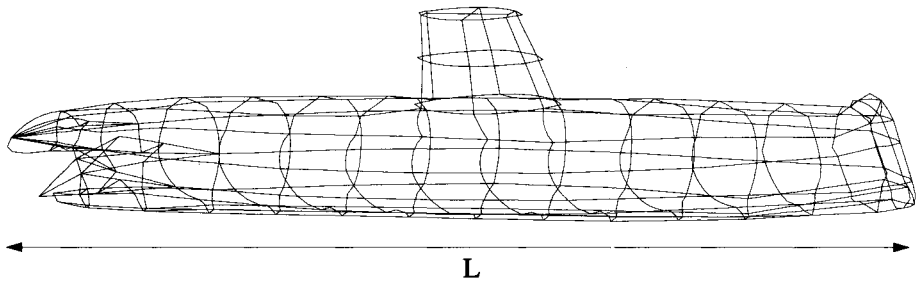

Figure 4. Submarine structure.

Table I. Point-source check of the submarine structure at $F/2$.

	MSE (%)		MSE (%)
option 1:	3	option 2:	3.5

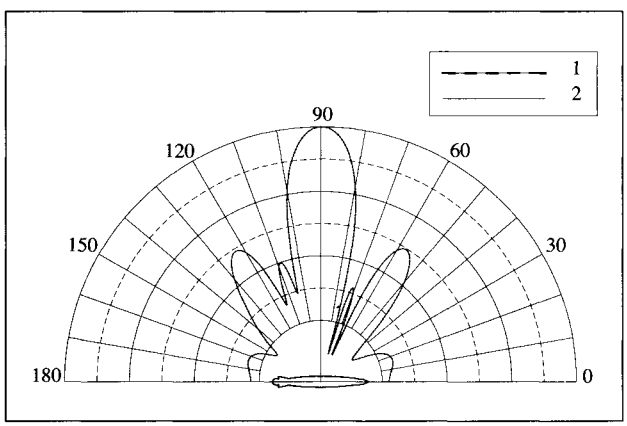

Figure 5. Rigid submarine monostatic far-field directivity pattern at $F/2$.

the surface. Then, the calculated pressure is compared to the analytical pressure by the Mean-Square Error (MSE):

$$\mathrm{MSE} = \sqrt{\frac{\sum_{n=1}^{N} \left|p_c(\boldsymbol{r}_n) - p_a(\boldsymbol{r}_n)\right|^2}{\sum_{n=1}^{N} \left|p_a(\boldsymbol{r}_n)\right|^2}}, \tag{19}$$

where N is the total number of nodes of the mesh, $p_c(\boldsymbol{r}_n)$ and $p_a(\boldsymbol{r}_n)$ respectively the calculated and the analytical pressure at the node n.

To validate this technique, numerous examples have been studied. Its illustration here is shown on a realistic structure: a submarine structure, which highest reduced frequency kL given by the "$\lambda/4$ criterion" is 30 (see Figure 4). The point-source check with the source situated at the centre of the structure at the frequency $F/2$ has shown (see Table I) the good behaviour of the interpolation computation between 0 and F (option 2) respected to the classical calculation (without using the interpolation technique) (option 1). The monostatic directivity pattern is drawn at frequency $F/2$ on Figure 5 where the classical calculation (option 1) is also compared to the interpolated computation between 0 and F (option 2).

The calculation frequency $F/2$ is the most unfavourable frequency, since it is the farthest from 0 and F. Nevertheless, the compliance between the two options is perfect. However, the costs of CPU time for the two options are equivalent.

5. Application to axisymmetrical problems

In this section, the application to the axisymmetrical case of the linear frequency interpolation technique is presented.

5.1. Theoretical application

For axisymmetrical problems, the elements used in the discretization of the equations are circular slices obtained by sub-divisions of the generatrix. These elements are isoparametric with quadratic variation and are constituted of 3 nodes [20] (see Figure 2). The form functions of these elements are:

$$\begin{aligned} N_1(\xi) &= \frac{1}{2}\xi(\xi - 1), \\ N_2(\xi) &= 1 - \xi^2, \\ N_3(\xi) &= \frac{1}{2}\xi(\xi + 1). \end{aligned} \tag{20}$$

The integrals in the HIE are evaluated via a semi-analytical method [21]. This integration method first consists in separating the singular parts (which appear when the calculation node r_m belongs to the element Γ_j in the equations (8), (9), (10) and (11)) in the Green's function and its normal derivative:

$$\frac{\mathrm{e}^{\mathrm{i}kD_m}}{D_m} = \frac{\mathrm{e}^{\mathrm{i}kD_m} - 1}{D_m} + \frac{1}{D_m} \tag{21}$$

$$\begin{aligned} &\frac{\mathrm{e}^{\mathrm{i}kD_m}}{D_m^2}\left(\mathrm{i}k - \frac{1}{D_m}\right) \\ &\quad = \frac{\mathrm{e}^{\mathrm{i}kD_m}(\mathrm{i}kD_m - 1) + 1}{D_m^3} - \frac{1}{D_m^3}. \end{aligned} \tag{22}$$

The integrands have been split into two parts (the singular and the non-singular). The non-singular integrals are calculated

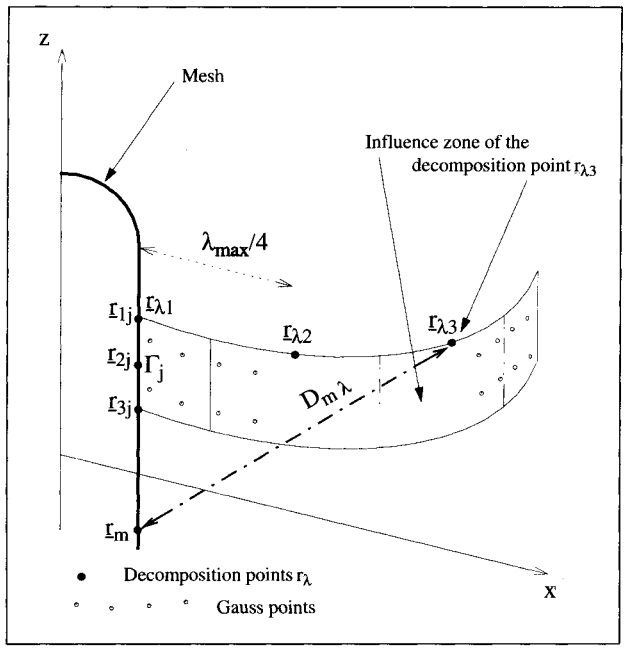

Figure 6. Axisymmetrical decomposition points and influence zones for the node $\boldsymbol{r}_{1j}$ of the element Γ_j.

by the Gauss-Legendre quadrature [20]. The treatment of singular integrals is based upon the use of elliptic integrals [22]: the numerical integration depending upon φ is removed and replaced by a series development of elliptic functions; the numerical integration depending upon ξ is done with the Gauss-Legendre numerical integration. Unfortunately, in (21) and (22), e^{ikD_m} cannot be factorised out in the two terms of the decomposition. Thus, referring to section 3.2., the linear frequency interpolation cannot be applied with this semi-analytical integration.

So, we propose another integration method which is compatible with the linear frequency interpolation principle. A complete numerical integration has been developed: the Gauss-Legendre quadrature on the two variables ξ and φ. Singularities appear when the calculation node r_m belongs to the element Γ_j. In this case and in order to treat this problem, the Gauss points number in the two directions ξ and φ is multiplied by 2 to increase the integration points density on the edge of the integration domain [23]. Therefore, the singularity in the neighbourhood of the local nodes 1 and 3 (see Figure 2) is suitably taken into account. However, when r_m is the local node 2, this increase of Gauss points is insufficient to treat the singularity with accuracy. Then, the integration domain of Γ_j is divided into two domains separated by node 2.

Many tests have allowed to underline that, for an equivalent convergence, this last integration method is faster (in CPU time) than the semi-analytical method.

Therefore, the linear frequency interpolation principle is applied with the complete numerical integration method. Such as in the 3D case, this principle is applied with the use of the distance $D_{m\,ij}$. In accordance with Figure 6, where a circular integration domain has been spread, some Gauss points can be located very far from the generatrix. Then $D_m - D_{m\,ij}$ can be very far from zero.

To be able to apply the linear frequency interpolation, we propose a decomposition of each circular element into subcircular elements. Every node of an element of the mesh belongs to a perimeter of a circle and a circular element covered by φ. The circular element is split into influence zones of the same length (see Figure 6). An influence zone is represented by a decomposition point $\boldsymbol{r}_\lambda$ of the perimeter of the node. This $\boldsymbol{r}_\lambda$ is the closest from all the Gauss points of its influence zone with regard to the others of the perimeter. So, at a given $\boldsymbol{r}$ of an element Γ_j, and a calculation node $\boldsymbol{r}_m$, for each influence zone, the factorisation (15) is done with the distance $D_{m\lambda}$ between $\boldsymbol{r}_m$ and its $\boldsymbol{r}_\lambda$. Thus, $D_m - D_{m\lambda}$ is small and the linear frequency interpolation scheme is led from end to end on each influence zone. After recovering the "original matrices" for all influence zones, a sum on all influence zones is done in order to obtain the complete integration.

Obviously, the decomposition points number has to be sufficient. Due to the kind of element used here, a $\lambda/4$ interval between the decomposition points is natural. To have the same decomposition points number for every interpolation frequency, an interval of $\lambda_{\max}/4$ is chosen ($\lambda_{\max} = c/F$ where c is the sound speed). Many tests have proven the convergence of this choice.

Here, for an axisymmetrical problem, with these quadratic elements, the "$\lambda/4$ criterion" also has to be verified and a projection of the right-hand matrix is done.

The disk storage space taken up by the bounding matrices is not cumbersome since the nodes are restricted to the generatrix.

5.2. Validation

The application of the linear frequency interpolation method to axisymmetrical problems presented in this paper is now tested and validated.

Four types of computations are presented:

- option a: semi-analytical option, issued from a classical calculation (without frequency interpolation) with the semi-analytical integration mode,
- option b: numerical option, issued from a classical computation with the complete numerical integration method,
- option c1: 1 interval option, issued from the linear frequency interpolation method with bounding frequencies equal to 0 and F,
- option c2: 2 intervals option, issued from the linear frequency interpolation method with two frequency intervals: 0–$F/2$ and $F/2$–F. In this case, three storages are executed, at 0, $F/2$ and F.

Several axisymmetrical examples are given to demonstrate the good behaviour of the BEM linear frequency interpolation technique and the improvement of computational efficiency (saving of CPU time).

The first three examples involve the point-source check described above. Comparisons are made between all the com-

ACUSTICA · acta acustica
Vol. 84 (1998)

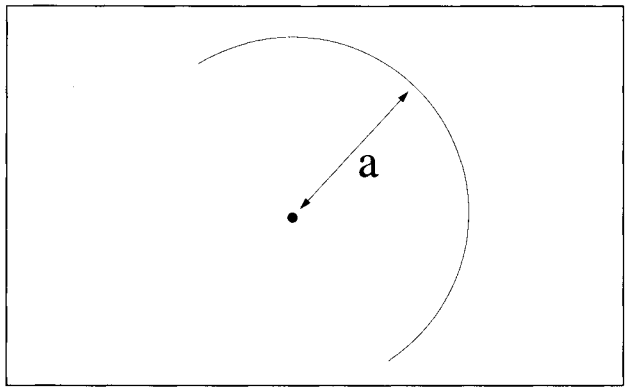

Figure 7. Sphere with the point-source at its centre.

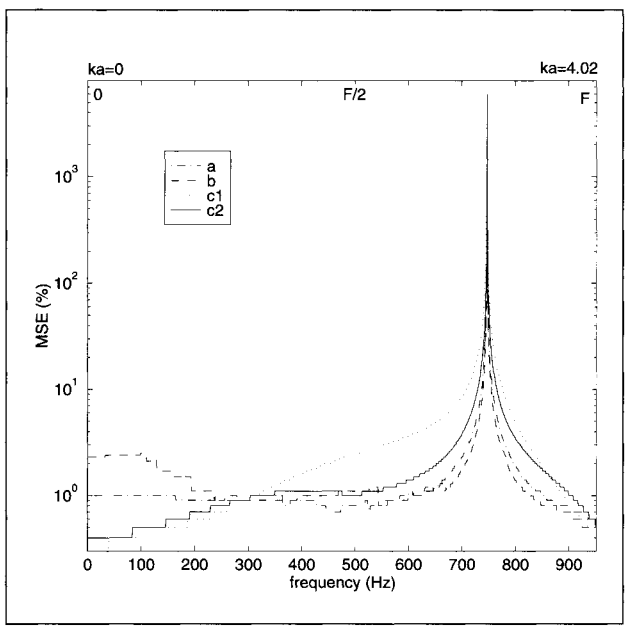

Figure 8. MSE for the sphere with 1 point-source at O.

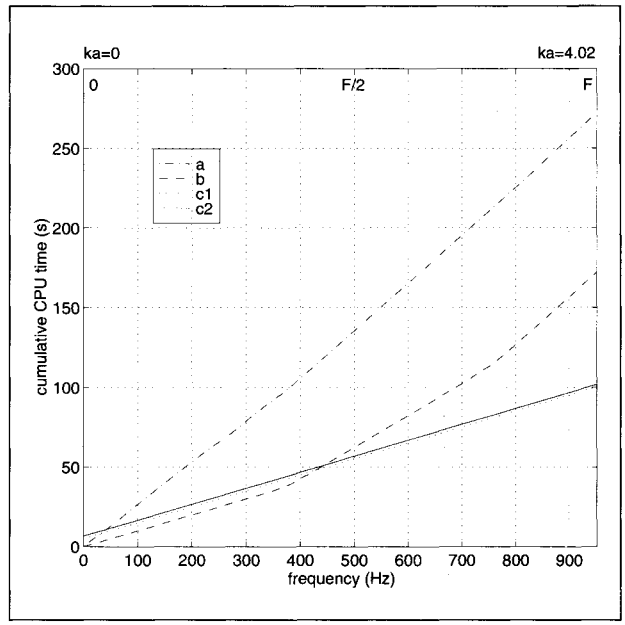

Figure 9. Cumulative CPU time for the sphere with 1 point-source at O.

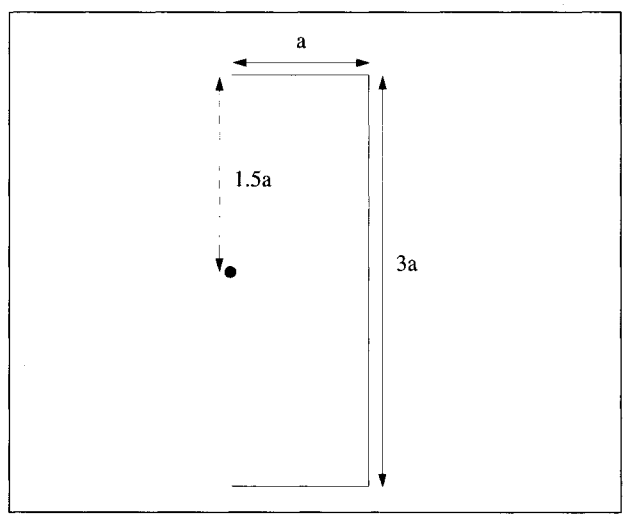

Figure 10. Cylinder with the point-source at its centre.

putation options. The whole frequency range is covered Hertz by Hertz.

The first structure is a sphere with maximum reduced frequency ka of 4.02 (see Figure 7). The point-source is situated at the centre of the structure. Figure 8 shows the logarithmic variation of the MSE versus frequency. Good agreement between all the options is observed. The irregular frequency is underlined for every option, but with a peak which is a little bit larger for option c1. Nevertheless, this relative imprecision is increased by the logarithmic scale used, which amplifies the weak differences. At a given calculation frequency, the cumulative CPU time takes into account the cost of CPU time of all the previous calculation frequencies of the range. Moreover, in the case of interpolation, the cost of CPU time of the storage steps is taken into account before the first calculation frequency. This cumulative CPU time is drawn versus frequency on Figure 9. The interpolation options become attractive from a number of calculation frequencies greater than the half of the total frequency number between 0 and F. The difference in CPU time between the two interpolation options is only due to the additional storage at $F/2$ when option c2 is used.

The second example is given on a cylinder (see Figure 10). The maximum ka is 6.28. The point-source is at the centre. Again, the MSE (see Figure 11) and cumulative CPU time (see Figure 12) versus frequency are provided. The conclusions are the same: good compliance between all the options, larger gap of the irregular frequency peaks with the interpolation technique option c1 and a good saving of CPU time, even clearer than on Figure 9, for the interpolation methods.

In the third example, the point-source is shifted from the centre of a structure usually called LINE (see Figure 13). The maximum ka of which is 7.85. With the LINE structure, the EQI code has already allowed computations for reduce wave

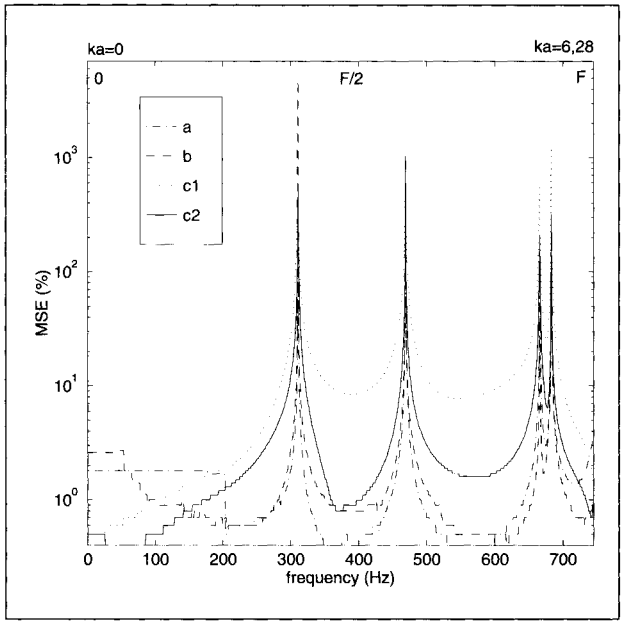

Figure 11. MSE for the cylinder with 1 point-source at O.

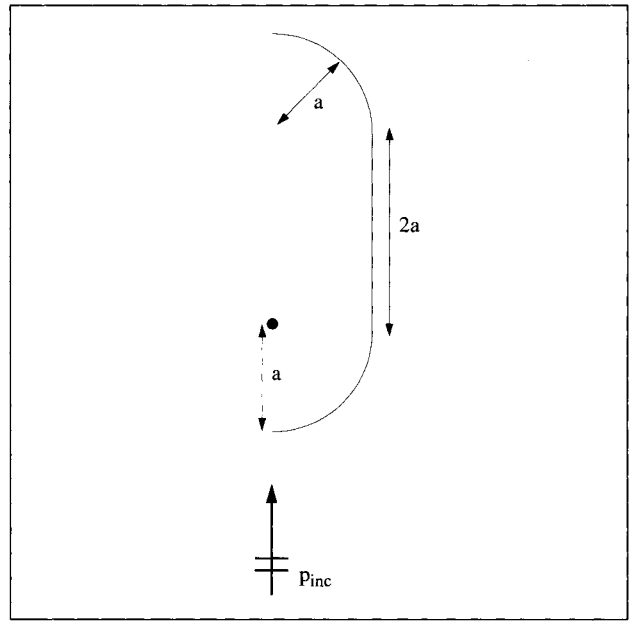

Figure 13. LINE with the point-source shifted from its centre and the incident plane wave.

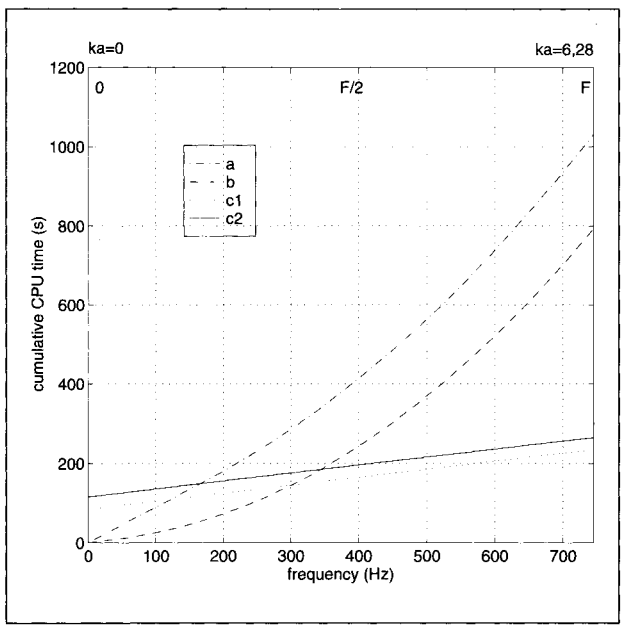

Figure 12. Cumulative CPU time for the cylinder with 1 point-source at O.

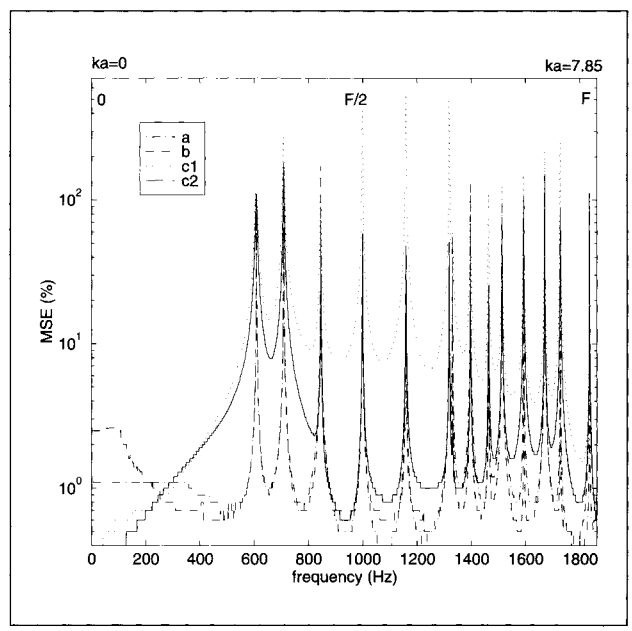

Figure 14. MSE for the LINE with 1 point-source shifted from the centre.

numbers of about 20 in 3D problems and 100 in axisymmetrical problems. The drawings of the MSE (see Figure 14) and cumulative CPU time (see Figure 15) versus frequency confirm the effectiveness of the linear interpolation method. In this case, the interpolation process needs about 5 times less CPU time to compute the whole frequency range than the classical methods.

The last example involves the scattering from the same LINE target, rigid, impinged by an incident plane wave travelling along the symmetrical axis of the geometry (see Figure 13). Figures 16 and 17 show the rigid backscattered normalized pressure spectrum. The computations are made at each frequency Hertz by Hertz. The scattered pressure modulus is normalized by the incident pressure modulus. On Figure 16, the pressure is calculated on the surface: the agreement between all the options is perfect, irregular frequencies are perfectly recovered; here, the trifling differences on the MSE does not exist anymore. In the far-field, the curves on Figure 17 show the great efficiency of the interpolation process.

ACUSTICA · acta acustica
Vol. 84 (1998)

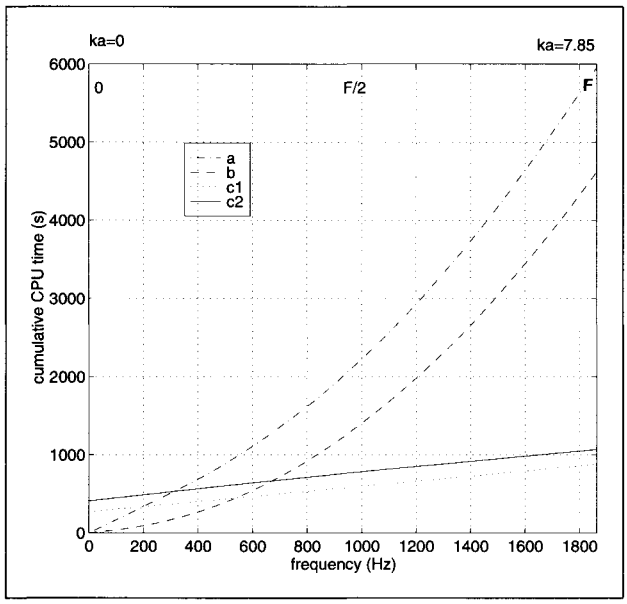

Figure 15. Cumulative CPU time for the LINE with 1 point-source shifted from the centre.

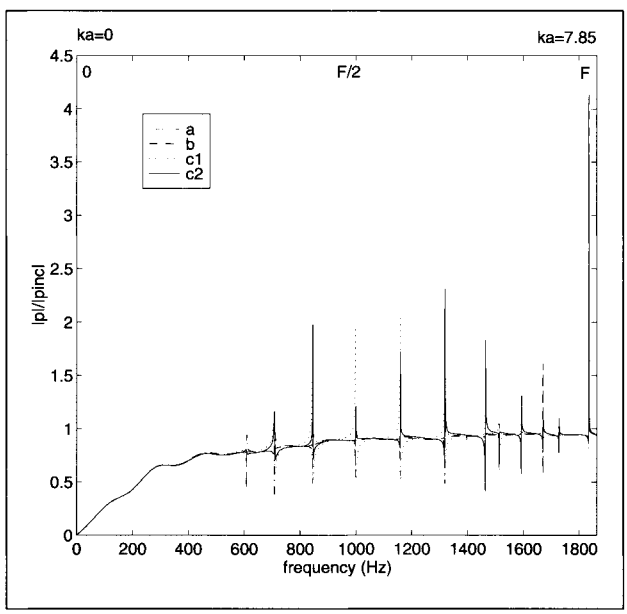

Figure 16. Rigid backscattered normalized pressure spectrum on the surface of line.

Figures 18, 19 and 20 show the far-field directivity pattern at three frequencies, respectively $F/4$, $F/2$ and $3F/4$. For option c2: at $F/4$, the interpolation process is done between 0 and $F/2$; at $F/2$, this calculation frequency being a bounding frequency, no interpolation is led; at $3F/4$, the interpolation process is done between $F/2$ and F. At the three frequencies, the curves are identical. Excellent agreement is again observed between every option.

The most important feature of the linear frequency interpolation method applied to axisymmetrical problems is certainly the saving of CPU time for a multi-frequency run without significant loss of accuracy. When the size of the

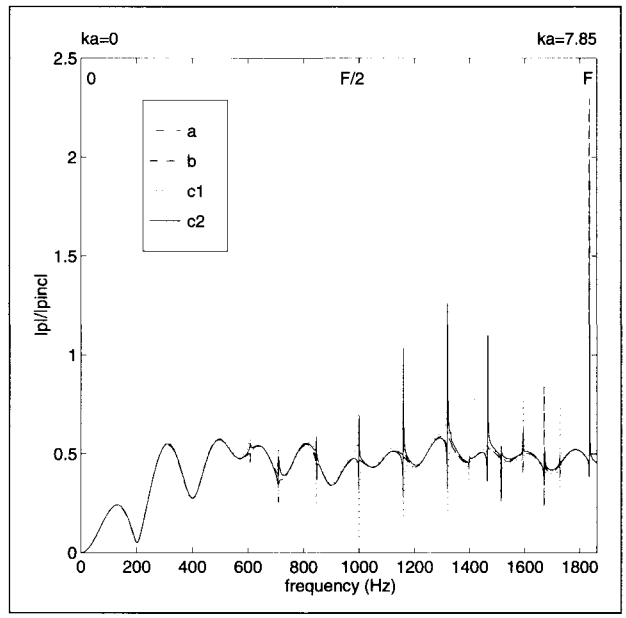

Figure 17. Far-field rigid backscattered normalized pressure spectrum.

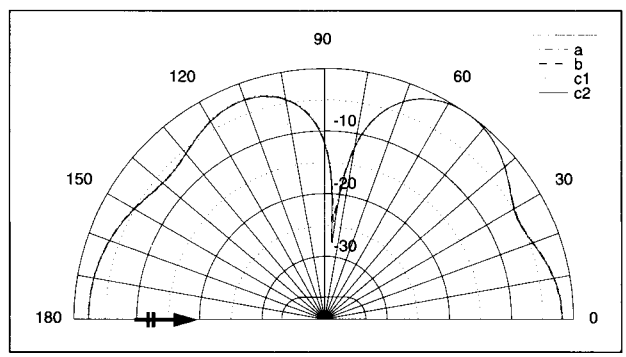

Figure 18. Far-field directivity pattern of rigid LINE at $F/4$ with incident plane wave travelling along the symmetrical axis.

mesh grows, the cost of CPU time during the interpolation step does not increase as much as the classical matrix construction phase. For this reason, as it has been observed on the Figures of cumulative CPU time, this technique becomes more and more attractive when the size of the mesh grows.

6. Conclusions

A linear frequency interpolation method has been developed for multi-frequency analysis in acoustics in the case of 3D and axisymmetrical problems. It is based upon a discretization with quadratic isoparametric elements of the HIE. This technique is very accurate when applied to 3D and axisymmetrical problems. For a multi-frequency run, in the case of 3D modelling, this method does not provide saving of CPU time. However, in the case of axisymmetrical modelling, it provides an important saving of CPU time. This saving becomes more important when the size of the mesh gets bigger. The very good behaviour of the axisymmetrical case is due

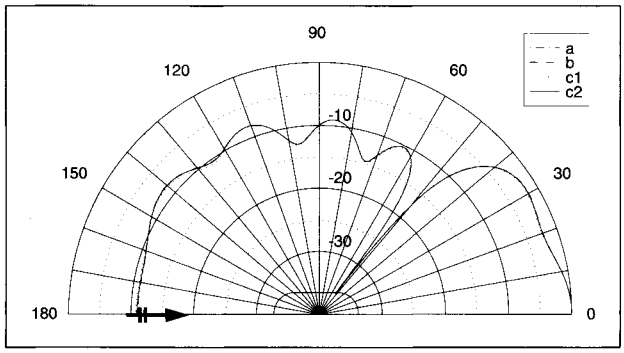

Figure 19. Far-field directivity pattern of rigid LINE at $F/2$ with incident plane wave travelling along the symmetrical axis.

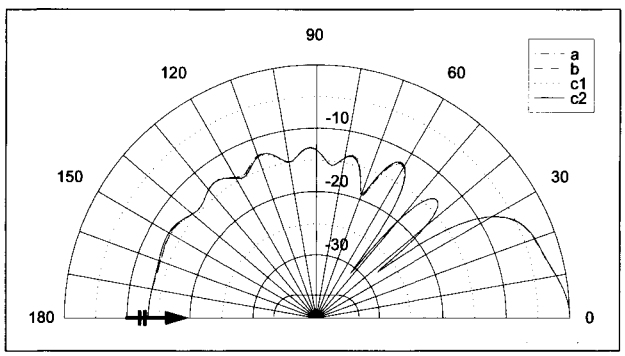

Figure 20. Far-field directivity pattern of rigid LINE at $3F/4$ with incident plane wave travelling along the symmetrical axis.

to the implementation of an original and automatic decomposition of the integration domain and an adapted integration method.

The application of the Jones method to the BEM interpolated system as well as its integration into the EQI-ATILA codes fluid-structure coupling is available but not presented here because of the perfect similarity of the results between classical and interpolation methods.

In conclusion, the BEM linear frequency interpolation technique presented in this paper turns out to be an efficient numerical tool to analyse multi-frequency acoustic scattering or radiation axisymmetrical problems.

Acknowledgement

The authors would like to thank J.R. Hartmann (DGA Toulon) and B. Poirée (DGA Paris) for their support for several years.

References

[1] J. N. Decarpigny: Application de la méthode des éléments finis à l'étude de transducteurs piézoélectriques. Dissertation. Université des Sciences et Techniques de Lille, 1984.

[2] J. N. Decarpigny, J. C. Debus, B. Tocquet, D. Boucher: In-air analysis of piezoelectric Tonpilz transducers in a wide frequency band using a mixed finite element-plane wave method. J. Acoust. Soc. Am. **78** (1985) 1499–1507.

[3] B. Stupfel, A. Lavie, J. N. Decarpigny: Combined integral equation formulation and null-field method for the exterior acoustic problem. J. Acoust. Soc. Am. **83** (1988) 927–941.

[4] A. Lavie: Modélisation du rayonnement ou de la diffraction acoustique par une méthode mixte équations intégrales-champ nul. Dissertation. Université des Sciences et Techniques de Lille, Flandres-Artois, 1989.

[5] A. Lavie, B. Hamonic, J. N. Decarpigny, D. Boucher: Modélisation du rayonnement ou de la diffraction acoustique de transducteurs basse fréquence à l'aide de la méthode des équations intégrales. Premier Congrès Français d'Acoustique, Supplément au Colloque de Physique, Colloque C2, Tome 51, 1990. 341–344.

[6] A. Lavie, B. Dubus: Modélisation de la diffraction acoustique d'une onde incidente plane par une structure élastique à l'aide d'une méthode mixte éléments finis-équations intégrales. Deuxième Congrès Français d'Acoustique, Supplément au Journal de Physique III, Colloque C1, Vol. 2, 1992. 957–960.

[7] D. Decultot, F. Lecrocq, G. Maze, J. Ripoche, B. Dubus, A. Lavie: Resonance interpretation with surface waves propagating on cylindrical shells bounded by hemispherical endcaps. Ultrasonics International 93 Conference Proceedings, Butterworth, 1993. 479–482.

[8] B. Dubus, A. Lavie, D. Decultot, G. Maze: Coupled finite element/boundary element method for the analysis of the acoustic scattering from elastic structures. ASME 15th bienal conference on vibration and noise, Acoustics of submerged structures and transduction for systems, 1995. Vol. 3 Part B, 25–32.

[9] A. Lavie, B. Dubus: Coupled finite element-boundary element method for scattering problems by axisymmetric bodies at oblique incidence. Proceedings of the 4th Congress on Acoustics, Vol. 2, 1997. 801–804.

[10] B. Dubus, A. Lavie, N. D. Veksler: A frequency derivative approach for identification of wave resonances on immersed elastic bodies. J. Acoust. Soc. Am. **102** (1997) 3523–3529.

[11] H. A. Schenck: Improved integral formulation for acoustic radiation problems. J. Acous. Soc. Am. **44** (1968) 41–58.

[12] L. G. Copley: Fundamental results concerning integral representations in acoustic radiation. J. Acous. Soc. Am. **44** (1967) 41–58.

[13] D. S. Jones: Integral equation for the exterior acoustic problem. Q. J. Mech. Appl. Math. **XXVII** (1974) 129–142.

[14] G. W. Benthien: Application of frequency interpolation to acoustic-structure interaction problems. Technical Report 1323, Naval Ocean Systems Center, San Diego, 1989.

[15] T. W. Wu, A. F. Seybert, G. C. Wan, R. D. Ciskowski: Vectorization and parallelization of the acoustic boundary element code BEMAP on the IBM ES/3090 VF. Proceedings, International Congress on Recent Developments in Air- and Structure-Borne Sound and Vibration, March 6-8 1990, Auburn University, Alabama, U.S.A., 1990. 489–498.

[16] C. Vanhille: Interpolation linéaire en fréquence appliquée à la méthode des équations intégrales. Diploma Thesis. Université des Sciences et Techniques de Lille, Flandres-Artois, 1991.

[17] T. W. Wu, R. D. Ciskowski, A. F. Seybert: Vectorization and parallelization of the acoustic boundary element code BEMAP on the IBM ES/3090 VF. Eng. Anal. Boundary Elements **10** (1992) 17–26.

[18] J. Giroire. Comptes rendus de la journée d'étude S.E.E. sur les calculs de propagation et de diffraction par la méthode des éléments finis, 1979.

[19] C. A. Brebbia, J. J. Rego Silva, P. W. Partridge: Boundary element methods in acoustics. Computational Mechanics Publications, Southampton Boston, 1991.

[20] O. C. Zienkiewics: The finite element method in engineering science. McGraw-Hill, Maidenhead, 1971.

[21] A. F. Seybert, B. Soenarko, F. J. Rizzo, D. J. Shippy: A special integral equation formulation for acoustic radiation and scattering for axisymmetric bodies and boundary conditions. J. Acoust. Soc. Am. **80** (1986) 1241–1247.

[22] I. S. Gradshteyn, I. M. Ryzhik: Table of integrals, series, and products. Academic Press, New York and London, 1965.

[23] M. Abramowitz, I. A. Stegun: Handbook of mathematical functions,. Dover Publications, New York, 1972.